Correspondence and
requests for materials
should be addressed to
Y.C.K. (yckang@
konkuk.ac.kr)

Electrochemical properties of cobalt hydroxychloride microspheres as a new anode material for Li-ion batteries

Gi Dae Park, You Na Ko & Yun Chan Kang

Department of Chemical Engineering, Konkuk University, 1 Hwayang-dong, Gwangjin-gu, Seoul 143-701, Korea.

The use of cobalt hydroxychloride [$Co_2(OH)_3Cl$] as an anode material for lithium ion batteries (LIBs) is investigated using spherical shape and ultrafine nanocrystals directly formed by spray pyrolysis from spray solution of cobalt chloride salt. Dot-mapping images of the resulting powders reveal a uniform distribution of Co, O, and Cl throughout the powder. The $Co_2(OH)_3Cl$ powder prepared directly by spray pyrolysis exhibits a high thermal stability at temperatures below 220°C, as well as having superior electrochemical properties compared with those of the $CoCl_2(H_2O)_2$ and CoO powders prepared by the same process. The initial discharge capacities of the $Co_2(OH)_3Cl$ and CoO powders at a constant current density of 1000 mA g^{-1} are found to be 1570 and 1142 mA h g^{-1}, respectively, and their initial Coulombic efficiencies are 72 and 70%. The discharge capacities of the $Co_2(OH)_3Cl$ and CoO powders after 100 cycles are 955 and 632 mA h g^{-1}, respectively. The $Co_2(OH)_3Cl$ powders have a high discharge capacity of 609 mA h g^{-1} even after 1000 cycles at a high current density of 5000 mA g^{-1}.

The high energy density of lithium ion batteries (LIBs) makes them suitable for various applications, ranging in size from portable electronic devices to zero-emission vehicles, but existing LIB technology is rapidly reaching its limits in terms of energy density (per volume) and specific energy (per weight)[1–3]. At present, graphitic materials are widely used as the anode material in lithium-ion batteries, mostly due to their low price and high reversibility. However, graphitic anodes inherently exhibit a relatively low capacity value (theoretical value equal to 372 mA h g^{-1}), and are thus inadequate for high power applications[4–7]. In order to ensure the successful use of Li-ion batteries in a wider variety of applications, for example electric cars, it is imperative to overcome at least some of the challenges related to obtaining a higher energy density, longer cycle life, improved high rate capability and greater safety[8–13]. A great deal of attention has therefore been focused on the anode materials used, as there is significant potential in this area for greatly improving battery performance[2,14–19]; the use of a more suitable anode material being by far the most effective means of achieving a high performance. To this end, metal oxides, sulfides, nitrides, fluorides, and oxysulfides have all been extensively explored as potential anode materials for lithium ion batteries[20–29]; their attraction being their ability to store excess lithium ions by a conversion reaction that results in a significantly larger reversible capacity than graphite.

Recently, copper hydroxychloride [$Cu_2Cl(OH)_3$] was studied as a promising anode material for LIBs[30], this material being able to reversibly store and release Li ions via a conversion reaction that is widely observed in CuO and CuS electrodes. The discharge capacities of chemically synthesized $Cu_2Cl(OH)_3$ powders at a low current density of 100 mA g^{-1} were found to be 1100 and 430 mA h g^{-1} for the 1st and 20th cycles, respectively. Moreover, although copper based materials containing CuO and CuS have poor electrochemical properties compared with the other transition metal-based materials such as Co, Mn, and Fe; metal hydroxychlorides excluding copper have not been studied as potential electrode materials for LIBs to the best of the authors' knowledge[20–23,31–33].

Cobalt basic salts, expressed using a general formula of $Co(OH)_{2-x}(A^{n-})_x$ (A: Cl^-, NO_3^-, SO_4^{2-}, CO_3^{2-}, etc.), have been extensively studied over the last two decades because of the important electric, magnetic, and catalytic properties of the metal oxides formed upon their thermal decomposition[34–37]. However, the preparation process to obtain cobalt basic salts with controlled morphologies, and their resulting electrochemical properties, have not been reported. In this study, cobalt hydroxychloride [$Co_2(OH)_3Cl$] is therefore studied for the first time as a potential anode material for LIBs. The spherical shape of $Co_2(OH)_3Cl$ powders produced by a simple one-pot spray pyrolysis process is found to result in superior electrochemical properties. Furthermore, the discharge capacity of bare $Co_2(OH)_3Cl$ powders, i.e., without carbonaceous materials generally improve the electrical

conductivity as well as acting as buffer layer for large volume changes during cycling, was high as 609 mA h g^{-1} after 1000 cycles at a high current density of 5000 mA g^{-1}.

Results

The crystal structures of the powders were found to be strongly affected by their respective preparation temperatures, as shown in Figure 1. Those powders prepared at temperatures of 500 and 900°C had primary crystal structures of $CoCl_2(H_2O)_2$ and CoO, respectively; however, the XRD pattern of the powders prepared directly by spray pyrolysis at 700°C indicated main peaks of $Co_2(OH)_3Cl$ crystals, and minor peaks of $CoCl_2(H_2O)_2$ and CoO crystals. Decomposition of $Co_2(OH)_3Cl$ into CoO was found to occur at a high preparation temperature of 900°C under a nitrogen atmosphere; and consequently, the optimum direct preparation temperature for $Co_2(OH)_3Cl$ powders by spray pyrolysis is located somewhere between 500 and 900°C.
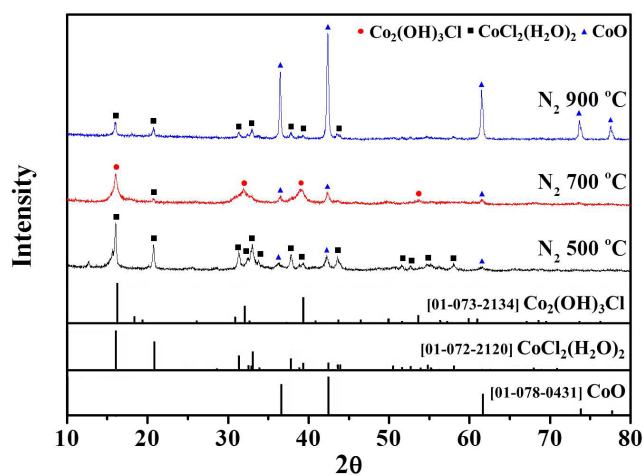
The $Co_2(OH)_3Cl$ powders prepared directly by spray pyrolysis at 700°C were found to have a spherical shape and porous structure, as shown by the SEM and TEM images in Figures 2a–2d. Moreover, the high resolution TEM image in Figure 2e shows the presence of ultra-fine nanocrystals of less than 10 nm in size, with clear lattice fringes separated by 0.59 and 0.42 nm. The dot-mapping images of the powders, as shown in Figure 2f, reveal a uniform distribution of Co, O, and Cl throughout the powder. The $Co_2(OH)_3Cl$ powder exhibiting both a spherical shape and ultrafine nanocrystals was directly formed from a single droplet of cobalt chloride salt by means of drying and decomposition.

Figures 3a and 3b show the EDX spectrum and thermogravimetric (TG) curve, respectively, for $Co_2(OH)_3Cl$ powders prepared directly by spray pyrolysis at 700°C. The respective concentrations of Co, O, and Cl were determined from the EDX spectrum as 45.4, 29.1, and 25.5 atomic%; and the mole ratio of the $Co_2(OH)_3Cl$ and $CoCl_2(H_2O)_2$ phases was estimated at 0.92 : 0.08 when the CoO content of the powders was ignored. The TG curve for the powders measured under air atmosphere exhibited three distinct weight losses below 1200°C; the reaction occurring with each decrease in weight being described in Figure 3b and summarized as follows: The first weight loss occurs below 380°C, and is due to the oxidation of $Co_2(OH)_3Cl$ to form $CoCl_2$, CoO_3, and H_2O[34]; the second weight loss occurs between 400 and 600°C, due to the decomposition of $CoCl_2$ into Co_3O_4[38]; and the final weight loss occurs above 1100°C, due to the reduction of Co_3O_4 into CoO[39]. Despite this, the cobalt hydroxychloride prepared directly by spray pyrolysis had high thermal stability at temperatures below 220°C. Figure S1a shows the N_2 adsorption and desorption isotherms of the powders prepared by

spray pyrolysis of a solution containing cobalt chloride at various temperatures, in which the hysteresis loops resemble the type-H3 IUPAC (International Union of Pure and Applied Chemistry) isotherm classification. The pore size distributions, as shown in Figure S1b, indicate that the powders have a mesoporous structure irrespective of their preparation temperature. The BET surface areas of the powders prepared at 500, 700, and 900°C were subsequently determined as 13, 6, and 4 m^2 g^{-1}, respectively.

The electrochemical properties of those powders with primary crystal structures of $CoCl_2(H_2O)_2$, $Co_2(OH)_3Cl$, and CoO were investigated in the voltage range of 0.001–3 V vs. Li/Li$^+$. Figure 4a shows the resulting initial discharge and charge voltage profiles at a constant current density of 1000 mA g^{-1}, from which it can be seen that the CoO powders prepared at 900°C produce two plateaus in the first discharging process. The first of these plateaus, appearing near 0.9 V, is associated with lithium storage in CoO[40–42]; whereas the second plateau located near 0.6 V can be ascribed to the conversion reaction between CoO and Li[40–42]. The slope, which is observed in the voltage range between 0.5 and 0.01 V, can be attributed to the interaction between Co particles and the electrolyte to form a solid electrolyte interface layer[40–42]. Conversely, the $Co_2(OH)_3Cl$ powders with small amounts of $CoCl_2(H_2O)_2$ and CoO impurities produced several plateaus in the first discharging and charging profiles. Compositionally, $Co_2(OH)_3Cl$ is a solid solution of $Co(OH)_2$ and $CoCl_2$[43]; therefore, $Co_2(OH)_3Cl$ reacts with Li according to the following reactions: $CoCl_2 + 2\,Li^+ + 2\,e^- \leftrightarrows Co + 2\,LiCl$ and $Co(OH)_2 + 2\,Li^+ + 2\,e^- \leftrightarrows Co + 2\,LiOH$[44,45]. The subsequent conversion reaction of LiOH to Li_2O and LiH could be responsible for generating the additional discharge capacity[46]. As a result, the $Co_2(OH)_3Cl$ powders have a higher initial discharge capacity than CoO powders. Furthermore, the lithium insertion and extraction processes of $Co_2(OH)_3Cl$ powders occur by a conversion reaction similar to that of transition metal oxides, as suggested by Tarascon et al. and Hu et al.[9,46] In this, crystalline Co nanoclusters and amorphous-like LiCl and LiOH could be formed by reactions of $Co(OH)_2$ and $CoCl_2$ with Li in the first discharging process. The initial discharge capacities of the $Co_2(OH)_3Cl$ and CoO powders were found to be 1570 and 1142 mA h g^{-1}, respectively; while their initial Coulombic efficiencies were 72 and 70%. Conversely, those $CoCl_2(H_2O)_2$ powders prepared at a low temperature of 500°C had initial discharge and charge capacities of 1146 and 588 mA h g^{-1}; while their corresponding Coulombic efficiency was 51%. Figure 4b shows the cyclic voltammograms (CVs) of $Co_2(OH)_3Cl$ powders for the first 5 cycles, in which the change in the discharging processes clearly alters the cathodic peak positions during cycling. The main cathodic peaks for the first and second discharging processes were observed at 0.9 and 1.7 V, but were subsequently moved to the lower-voltage regions during subsequent cycles. The remarkable differences in potential between the first and subsequent discharge curves were also observed, as shown in Figure S2. These results indicate that the original structure of the $Co_2(OH)_3Cl$ cannot be reversibly recovered after the first discharge process.

Figure 4c shows the cycling performances of the powders prepared at various temperatures at a constant current density of 1000 mA g^{-1}. The discharge capacities of those powders prepared at 700°C, and having a primary crystal structure of $Co_2(OH)_3Cl$, decreased from 1570 to 872 mA h g^{-1} for the first 8 cycles; but then slightly increased to 955 mA h g^{-1} during the subsequent 93 cycles. This initial decrease in the discharge capacities (2–7 cycles) was related to the transformation of the crystalline structure to a stable amorphous-like structure during cycling[47,48]. On the other hand, the discharge capacities of those powders prepared at 900°C, with a primary crystal structure of CoO, decreased steadily from 1142 to 632 mA h g^{-1} over 100 cycles. Additionally, the $Co_2(OH)_3Cl$ powders with ultrafine crystallite sizes are shown to have better cycling performance than CoO powders with a high crystallinity. The

Figure 1 | XRD patterns of the powders prepared by spray pyrolysis at various temperatures.
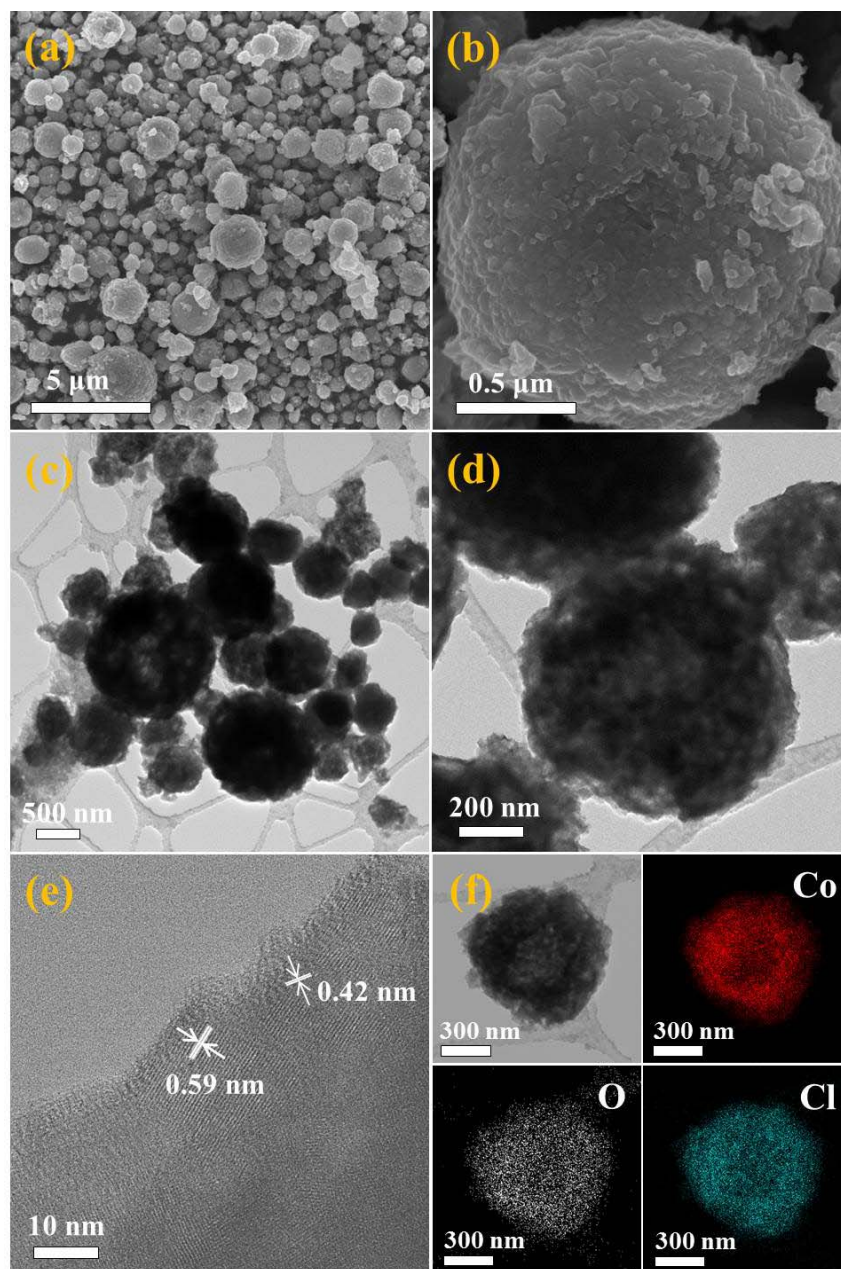
Figure 2 | Morphologies and dot-mapping images of the $Co_2(OH)_3Cl$ powders prepared at 700°C: (a) and (b) SEM images, (c) and (d) TEM images, (e) high resolution TEM image, and (f) dot-mapping images.

$CoCl_2(H_2O)_2$ powders prepared at a low temperature of 500°C had low discharge capacities of 1146 and 478 mA h g^{-1} for the 1st and 100th cycles, respectively. The Coulombic efficiencies of the $Co_2(OH)_3Cl$ powders reached above 99% from the 7th cycle at a current density of 1000 mA g^{-1} as shown in Figure 4c. The rate performance of the $Co_2(OH)_3Cl$ powders prepared at 700°C was demonstrated by the stepwise increase in Figure 4d from 500 to 5000 mA g^{-1} and the return to 500 mA g^{-1} in the voltage range of 0.001–3 V. For each step, 10 cycles were measured to evaluate the rate performance. The $Co_2(OH)_3Cl$ powders prepared at 700°C exhibited final discharge cycle capacities of 1039, 1001, 969, 936, 905, 879, 832, and 787 mA h g^{-1} at current densities of 500, 1000, 1500, 2000, 2500, 3000, 4000, and 5000 mA g^{-1}, respectively. When the current density returned to 500 mA g^{-1}, the discharge capacity recovered to 1063 mA h g^{-1} in spite of the cycling at high current densities, which indicates the good rate performance. Figure 4e shows the long-term cycling performance of the $Co_2(OH)_3Cl$ pow-

ders prepared at 700°C at a high current density of 5000 mA g^{-1}, from which the discharge capacities for the 2nd and 1000th cycles were determined as 818 and 609 mA h g^{-1}, respectively. The Coulombic efficiencies of the $Co_2(OH)_3Cl$ powders reached above 99% from the 15th cycle at a high current density of 5000 mA g^{-1} as shown in Figure 4e.

The Nyquist impedance plots obtained before and after the 1st and 100th cycles under a fully charged state for powders prepared at various temperatures are shown in Figure 5. In this, the medium-frequency semicircle is assigned to the charge-transfer resistance (R_{ct}), whereas the line inclined at ~45° to the real axis corresponds to the lithium diffusion process within the electrodes[49–51]. The diameter of the semicircle obtained for the $Co_2(OH)_3Cl$ powder electrode, before cycling in the medium-frequency region, was slightly smaller than those of the electrodes having primary crystal structures of CoO and $CoCl_2(H_2O)_2$ as shown in Figure 5a. Similarly, the charge-transfer resistance of the $Co_2(OH)_3Cl$ powder electrode was
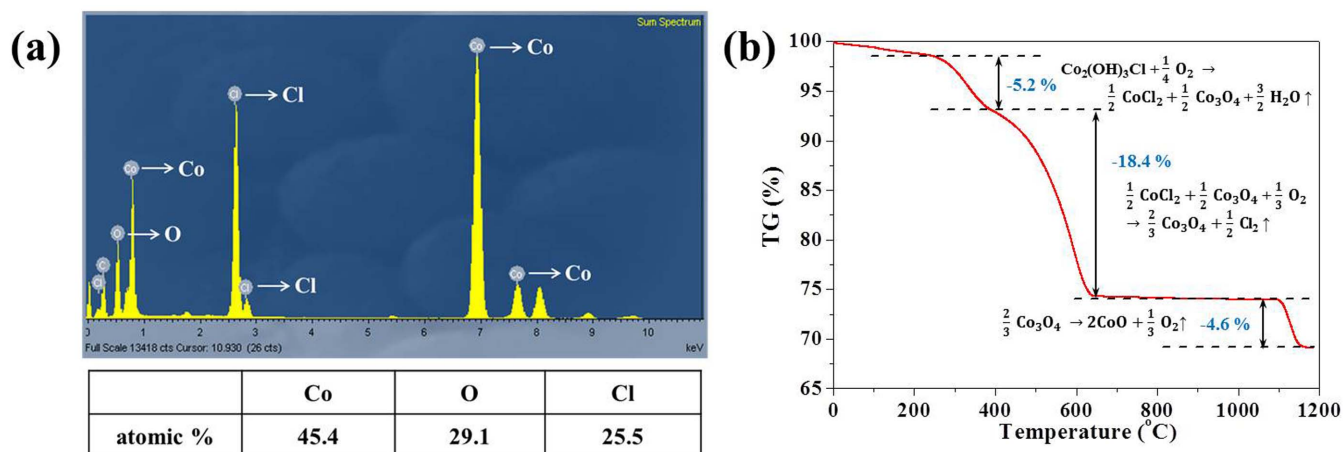
Figure 3 | (a) EDX spectrum and (b) TG curve of the $Co_2(OH)_3Cl$ powders prepared at 700°C.
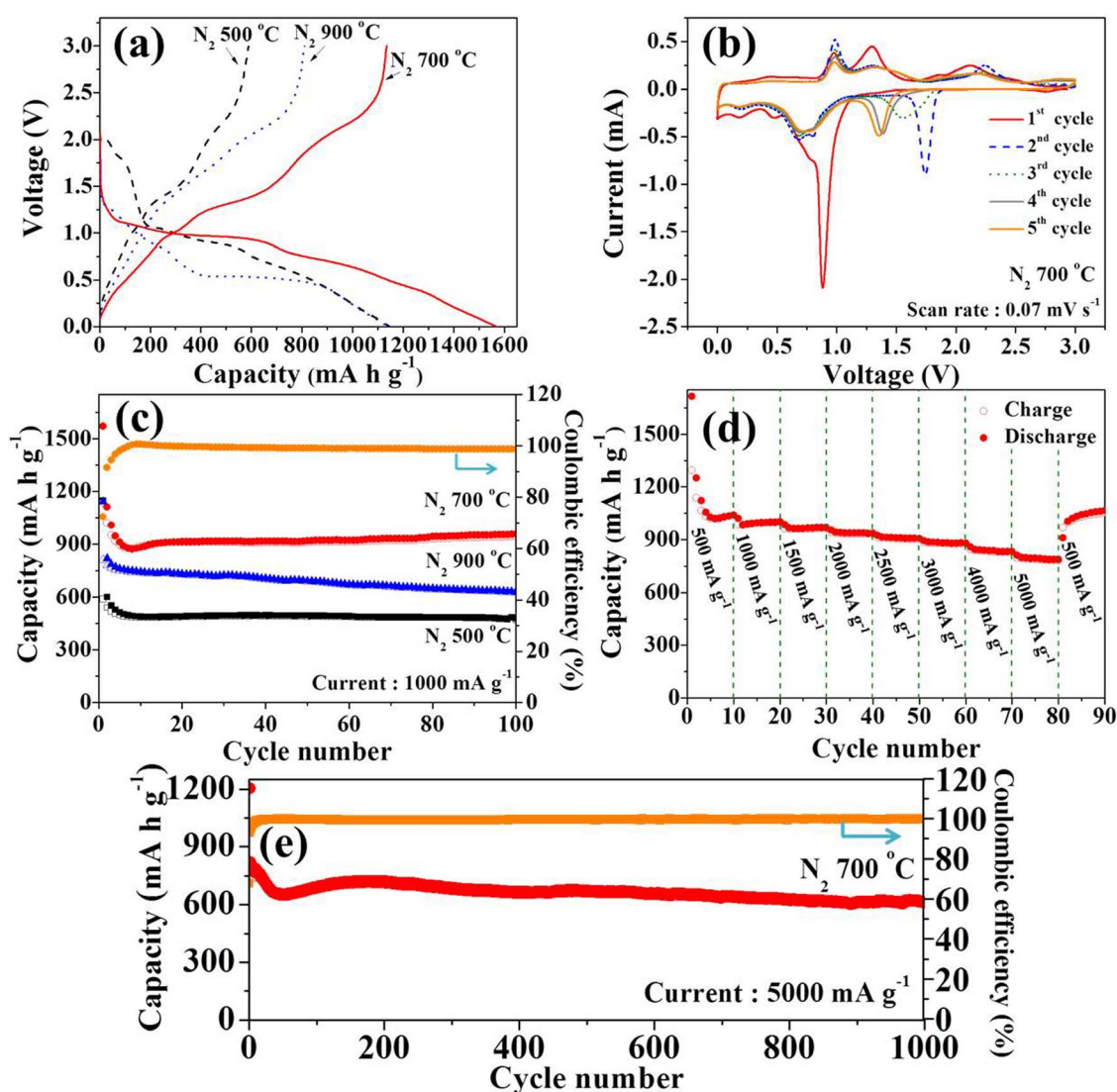

Figure 4 | Electrochemical properties of the powders prepared by spray pyrolysis at various temperatures: (a) initial discharge/charge voltage profiles at a constant current density at 1000 mA g^{-1}, (b) CVs of the $Co_2(OH)_3Cl$ powders, (c) cycling performances at a constant current density of 1000 mA g^{-1}, (d) rate performance of the $Co_2(OH)_3Cl$ powders, and (e) cycling performance of the $Co_2(OH)_3Cl$ powders at a high current density of 5000 mA g^{-1}.
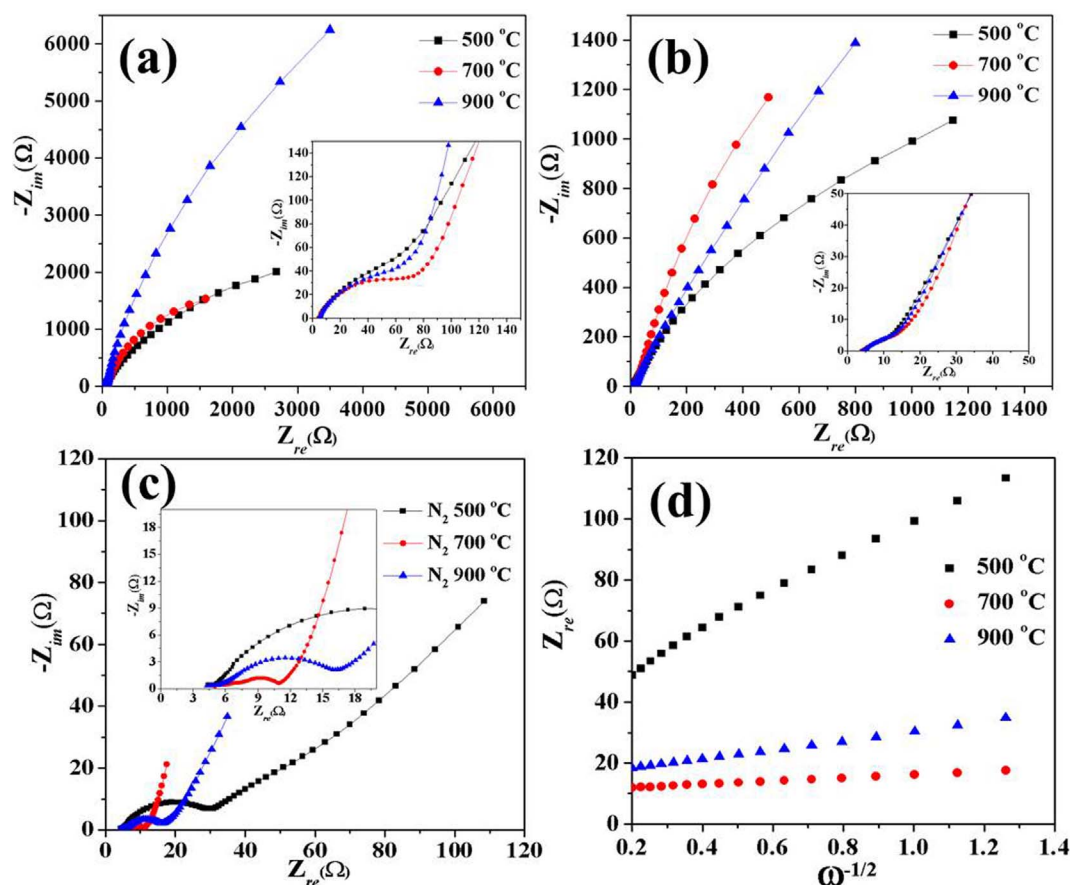
Figure 5 | Nyquist plots of the electrochemical impedance spectra of the powders prepared at various temperatures (a) before and after the (b) 1st and (c) 100th cycles and (d) relationship between the real part of the impedance spectra (Z_{re}) and $\omega^{-1/2}$ after 100 cycles.

smaller than those of the CoO and CoCl$_2$(H$_2$O)$_2$ powder electrodes. The electrodes having primary crystal structures of Co$_2$(OH)$_3$Cl, CoO, and CoCl$_2$(H$_2$O)$_2$ had similar charge-transfer resistances after first cycles as shown in Figure 5b. However, the diameter of the semicircle obtained for the Co$_2$(OH)$_3$Cl powder electrode, after 100th cycling in the medium-frequency region, was smaller than those of the CoO and CoCl$_2$(H$_2$O)$_2$ powder electrodes as shown in Figure 5c. The structural stability of the Co$_2$(OH)$_3$Cl powder resulted in the low charge transfer resistance even after 100 cycles. Figure 5d shows the relationship between the real part of the impedance spectra (Z_{re}) and $\omega^{-1/2}$ (where ω is the angular frequency in the low frequency region, $\omega = 2\pi f$) in the low-frequency region after 100 cycles. The lower slope (σ, Warburg impedance coefficient) of the real part of the impedance spectra (Z_{re}) versus $\omega^{-1/2}$ for the Co$_2$(OH)$_3$Cl powder electrode reveals a higher lithium-ion diffusion rate than CoO and CoCl$_2$(H$_2$O)$_2$ powder electrodes[52–54]. Figure 6 shows the morphologies of the Co$_2$(OH)$_3$Cl powders obtained after 100th charging process. The TEM image as shown in Figure 6a shows that the spherical morphology of the Co$_2$(OH)$_3$Cl powder was maintained even after repeated charging and discharging processes. However, the powders had amorphous-like structure after cycling. The high resolution TEM image as shown inset image in Figure 6c shows the lattice fringes with a separation of 0.29 nm, which corresponds to the (300) lattice plane of α-Co(OH)$_2$. The structural stability and high lithium ion diffusion rate of the Co$_2$(OH)$_3$Cl powders resulted in superior electrochemical properties even at high current density.

Discussion

The Co$_2$(OH)$_3$Cl powders demonstrated good cycling and rate performances even without carbonaceous additives, which are usually
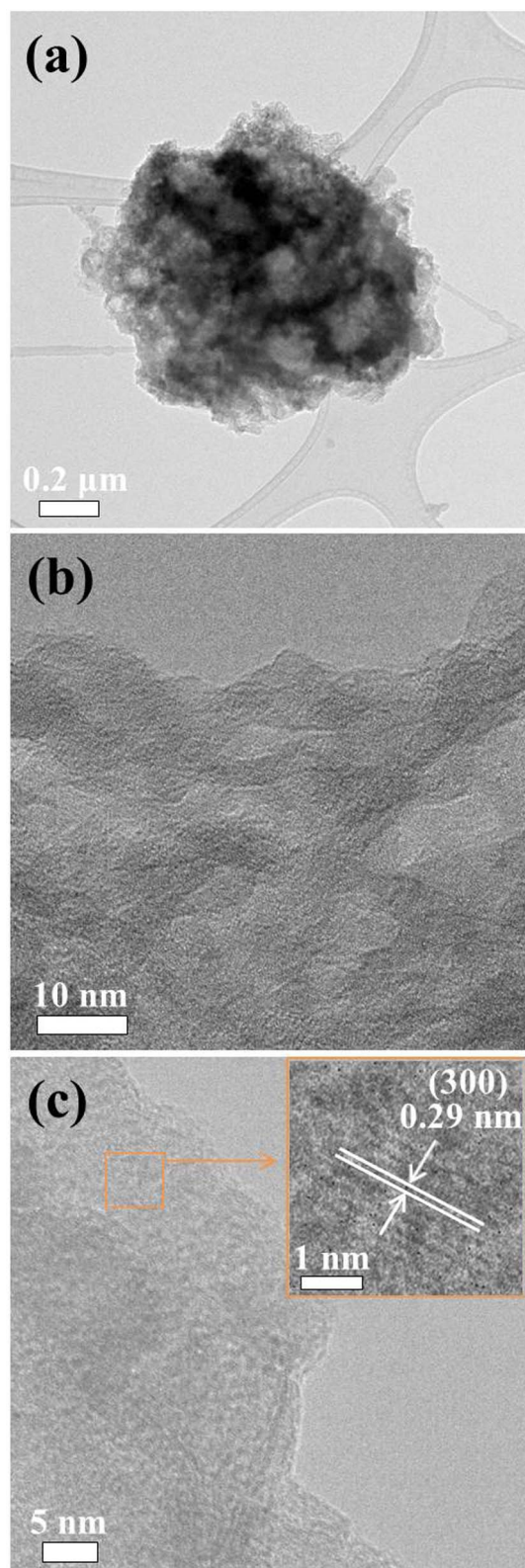
applied to improve the electrochemical properties of transition metal oxides. The pristine Co(OH)$_2$ powders prepared by the hydrothermal process had discharge capacities at a low current density of 200 mA g^{-1} of 1599 and 910 mA h g^{-1} for the 1st and 30th cycles, respectively[44]. Meanwhile, the pure CoCl$_2$ powders had respective discharge capacities of 850 and 400 mA h g^{-1} for the 1st and 50th cycles, at a low current density of 0.2 C[45]. The Co$_2$(OH)$_3$Cl powders introduced in this study therefore present a more promising anode material for LIBs than either CoCl$_2$ or Co(OH)$_2$.

The characteristics of cobalt hydroxychloride [Co$_2$(OH)$_3$Cl] prepared by a one-pot spray pyrolysis were investigated with a view to their potential application as an anode material for LIBs. Spray pyrolysis proved to be efficient for the direct preparation of Co$_2$(OH)$_3$Cl powders from a spray solution containing cobalt chloride under a nitrogen atmosphere. Moreover, Co$_2$(OH)$_3$Cl powders, which are a solid solution of Co(OH)$_2$ and CoCl$_2$, were found to have superior electrochemical properties than more well-known anode materials such as CoO, as well as individual CoCl$_2$ and Co(OH)$_2$ materials. It was also found that the electrochemical properties of Co$_2$(OH)$_3$Cl powders can be improved by optimizing the phase purity and crystallinity, as well as developing novel nanostructures. Therefore, although this is the first such study of Co$_2$(OH)$_3$Cl materials, they nonetheless show great promise as a potential anode material for LIBs.

Methods

Material fabrication. The Co$_2$(OH)$_3$Cl, CoCl$_2$(H$_2$O)$_2$, and CoO powders were prepared by one-pot spray pyrolysis from the spray solution of cobalt chloride by changing the preparation temperatures from 500 to 900°C under nitrogen atmosphere. The concentration of cobalt chloride was 0.15 M. The spray pyrolysis system consisted of a droplet generator, a high-temperature tubular quartz reactor,

Figure 6 | Morphologies of the Co₂(OH)₃Cl powders obtained after 100ᵗʰ charging process.

(FE-TEM, JEM-2100F). The crystal structures of the samples were investigated by X-ray diffractometry (XRD, X'Pert PRO MPD) using Cu Kα radiation (λ = 1.5418 Å) at the Korea Basic Science Institute (Daegu). Thermal gravimetric analysis (TGA, SDT Q600) was performed in air to determine the amount of carbon in the powders. The surface areas of the samples were measured by the Brunauer-Emmett-Teller (BET) method using N_2 as the adsorbate gas.

Electrochemical measurements. The electrochemical properties of the prepared powders were analyzed in a 2032-type coin cell. The anode was prepared from a mixture of the active material, carbon black, and sodium carboxymethyl cellulose (CMC) in a weight ratio of 7 : 2 : 1. Li metal and a microporous polypropylene film were used as the counter electrode and the separator, respectively. The electrolyte was 1 M $LiPF_6$ dissolved in a mixture of ethylene carbonate/dimethyl carbonate (EC/DMC; 1 : 1 v/v) with 2% vinylene carbonate. The discharge/charge characteristics of the samples were investigated through cycling in the 0.001–3 V potential range at various current densities. Cyclic voltammograms were measured at a scan rate of 0.07 mV s⁻¹.

1. McDowell, M. T., Lee, S. W., Nix, W. D. & Cui, Y. 25th anniversary article: understanding the lithiation of silicon and other alloying anodes for lithium-ion batteries. *Adv. Mater.* **25**, 4966–4985 (2013).
2. Reddy, M. V., Subba Rao, G. V. & Chowdari, B. V. R. Metal oxides and oxysalts as anode materials for Li ion batteries. *Chem. Rev.* **113**, 5364–5457 (2013).
3. Choi, N. S. *et al.* Challenges Facing Lithium Batteries and Electrical Double-Layer Capacitors. *Angew. Chem. Int. Ed.* **51**, 9994–10024 (2012).
4. Armand, M. & Tarascon, J. M. Building better batteries. *Nature* **451**, 652–657 (2008).
5. Winter, M., Besenhard, J. Q., Spahr, M. E. & Novák, P. Insertion electrode materials for rechargeable lithium batteries. *Adv. Mater.* **10**, 725–762 (1998).
6. Kaskhedikar, N. A. & Maier, J. Lithium storage in carbon nanostructures. *Adv. Mater.* **21**, 2664–2680 (2009).
7. Wang, C. S., Wu, G. T. & Li, W. Z. Lithium insertion in ball-milled graphite. *J. Power Sources* **76**, 1–10 (1998).
8. Tarascon, J. M. & Armand, M. Issues and challenges facing rechargeable lithium batteries. *Nature* **414**, 359–367 (2001).
9. Bruce, P. G., Scrosati, N. & Tarascon, J. M. Nanomaterials for rechargeable lithium batteries. *Angew. Chem. Int. Ed.* **47**, 2930–2946 (2008).
10. Etacheri, V., Marom, R., Elazari, R., Salitra, G. & Aurbach, D. Challenges in the development of advanced Li-ion batteries: a review. *Energy Environ. Sci.* **4**, 3243–3262 (2011).
11. Palacín, M. R. Recent advances in rechargeable battery materials: a chemist's perspective. *Chem. Soc. Rev.* **38**, 2565–2575 (2009).
12. Scrosati, B., Hassoun, J. & Sun, Y. K. Lithium-ion batteries. A look into the future. *Energy Environ. Sci.* **4**, 3287–3295 (2011).
13. Lu, L., Han, X., Li, J., Hua, J. & Ouyang, M. A review on the key issues for lithium-ion battery management in electric vehicles. *J. Power Sources* **226**, 272–288 (2013).
14. Poizot, P., Laruelle, S., Grugeon, S., Dupont, L. & Tarascon, J. M. Nano-sized transition-metal oxides as negative-electrode materials for lithium-ion batteries. *Nature* **407**, 496–499 (2000).
15. Ji, L., Lin, Z., Alcoutlabi, M. & Zhang, X. Recent developments in nanostructured anode materials for rechargeable lithium-ion batteries. *Energy Environ. Sci.* **4**, 2682–2699 (2011).
16. Wang, Z., Zhou, L. & Lou, X. W. Metal oxide hollow nanostructures for lithium-ion batteries. *Adv. Mater.* **24**, 1903–1911 (2012).
17. Wu, H. B., Chen, J. S., Hng, H. H. & Lou, X. W. Nanostructured metal oxide-based materials as advanced anodes for lithium-ion batteries. *Nanoscale* **4**, 2526–2542 (2012).
18. Lai, C. H., Lu, M. Y. & Chen, L. J. Metal sulfide nanostructures: synthesis, properties and applications in energy conversion and storage. *J. Mater. Chem.* **22**, 19–30 (2012).
19. Gao, M. R., Xu, Y. F., Jiang, J. & Yu, S. H. Nanostructured metal chalcogenides: synthesis, modification, and applications in energy conversion and storage devices. *Chem. Soc. Rev.* **42**, 2986–3017 (2013).
20. Wang, H. *et al.* Mn₃O₄-graphene hybrid as a high-capacity anode material for lithium ion batteries. *J. Am. Chem. Soc.* **132**, 13978–13980 (2010).
21. Li, Y., Tan, B. & Wu, Y. Mesoporous Co₃O₄ nanowire arrays for lithium ion batteries with high capacity and rate capability. *Nano Lett.* **8**, 265–270 (2008).
22. Zhang, W. M., Wu, X. L., Hu, J. S., Guo, Y. G. & Wan, L. J. Carbon coated Fe₃O₄ nanospindles as a superior anode material for lithium-ion batteries. *Adv. Funct. Mater.* **18**, 3941–3946 (2008).
23. Zhou, G. *et al.* Graphene-wrapped Fe₃O₄ anode material with improved reversible capacity and cyclic stability for lithium ion batteries. *Chem. Mater.* **22**, 5306–5313 (2010).
24. Varghese, B. *et al.* Fabrication of NiO nanowall electrodes for high performance lithium ion battery. *Chem. Mater.* **20**, 3360–3367 (2008).
25. Courtel, F. M., Duncan, H., Abu-Lebdeh, Y. & Davidson, I. J. High capacity anode materials for Li-ion batteries based on spinel metal oxides AMn₂O₄ (A = Co, Ni, and Zn). *J. Mater. Chem.* **21**, 10206–10218 (2011).
26. Yu, L., Zhang, L., Wu, H. B., Zhang, G. & Lou, X. W. Controlled synthesis of hierarchical CoₓMn₃₋ₓO₄ array micro-/nanostructures with tunable morphology

and a Teflon bag filter (powder collector). A 1.7-MHz ultrasonic spray generator having six vibrators was used to generate a large number of droplets, which were then carried to the quartz reactor by a carrier gas. The length and diameter of the quartz reactor were 1200 and 50 mm, respectively.

Characterization. The morphologies of the samples were investigated by scanning electron microscopy (SEM, JEOL JSM-6060) and transmission electron microscopy

and composition as integrated electrodes for lithium-ion batteries. *Energy Environ. Sci.* **6**, 2664–2671 (2013).

27. Mahmood, N., Zhang, C. & Hou, Y. Nickel sulfide/nitrogen-doped graphene composites: phase-controlled synthesis and high performance anode materials for lithium ion batteries. *Small* **9**, 1321–1328 (2013).

28. Wu, B., Song, H., Zhou, J. & Chen, X. Iron sulfide-embedded carbon microsphere anode material with high-rate performance for lithium-ion batteries. *Chem. Commun.* **47**, 8653–8655 (2011).

29. Choi, S. H. & Kang, Y. C. Synthesis for yolk-shell-structured metal sulfide powders with excellent electrochemical performances for lithium-ion batteries. *Small* **10**, 474–478 (2014).

30. Kim, S. W. *et al.* Energy storage in in vivo synthesizable biominerals. *RSC Adv.* **2**, 5499–5501 (2012).

31. Xiong, S., Chen, J. S., Lou, X. W. & Zeng, H. C. Mesoporous Co_3O_4 and CoO@C topotactically transformed from chrysanthemum-like $Co(CO_3)_{0.5}(OH)\cdot0.11H_2O$ and their lithium-storage properties. *Adv. Funct. Mater.* **22**, 861–871 (2012).

32. Chen, J. S. *et al.* Shape-controlled synthesis of Co_3O_4 nanostructures and their comparative lithium storage properties. *ACS Appl. Mater. Interfaces* **2**, 3628–3635 (2010).

33. Lou, X. W., Deng, D., Lee, J. Y. & Archer, L. A. Thermal formation of mesoporous single-crystal Co_3O_4 nano-needles and their lithium storage properties. *J. Mater. Chem.* **18**, 4397–4401 (2008).

34. García-Martínez, O., Millán, P., Rojas, R. M. & Torralvo, M. J. Cobalt basic salts as inorganic precursors of cobalt oxides and cobalt metal: thermal behaviour dependence on experimental conditions. *J. Mater. Sci.* **23**, 1334–1350 (1988).

35. Zheng, X., Kawae, T., Yamada, H., Nishiyama, K. & Xu, C. Coexisting ferromagnetic order and disorder in a uniform system of hydroxyhalide $Co_2(OH)_3Cl$. *Phys. Rev. Lett.* **97**, 274204 (2006).

36. Zheng, M. G., Hagihala, M., Fujihala, M. & Kawae, T. Recent developments in the magnetic study of the deformed pyrochlore lattice $M_2(OH)_3X$ (M = 3d magnetic ions, X = Cl, Br) - exotic magnetic order in $Ni_2(OH)_3Cl$ and controlled spin-spin interactions in $Co_2(OH)_3Cl_{1-x}Br_x$ and $(Co_{1-x}Fe_x)_2(OH)_3Cl$. *J. Phys.: Conf. Ser.* **145**, 012034 (2009).

37. Hu, Z. A. *et al.* Synthesis of α-cobalt hydroxides with different intercalated anions and effects of intercalated anions on their morphology, basal plane spacing, and capacitive property. *J. Phys. Chem. C* **113**, 12502–12508 (2009).

38. Wang, X. *et al.* Synthesis of single-crystalline Co_3O_4 octahedral cages with tunable surface aperture and their lithium storage properties. *J. Phys. Chem. C* **113**, 15553–15558 (2009).

39. Guo, Q., Guo, X. & Tian, Q. Optionally ultra-fast synthesis of CoO/Co_3O_4 particles using $CoCl_2$ solution via a versatile spray roasting method. *Adv. Powder Technol.* **21**, 529–533 (2010).

40. Chen, C. H. *et al.* An understanding of anomalous capacity of nano-sized CoO anode materials for advanced Li-ion battery. *Electrochem. Commun.* **12**, 496–498 (2010).

41. Peng, C. *et al.* Facile ultrasonic synthesis of CoO quantum dot/graphene nanosheet composites with high lithium storage capacity. *ACS Nano* **6**, 1074–1081 (2012).

42. Do, J. S. & Weng, C. H. Preparation and characterization of CoO used as anodic material of lithium battery. *J. Power Sources* **146**, 482–486 (2005).

43. Zhao, Z., Geng, F., Bai, J. & Cheng, H. M. Facile and controlled synthesis of 3D nanorods-based urchinlike and nanosheets-based flowerlike cobalt basic salt nanostructures. *J. Phys. Chem. C* **111**, 3848–3852 (2007).

44. He, Y. S. *et al.* A $Co(OH)_2-$graphene nanosheets composite as a high performance anode material for rechargeable lithium batteries. *Electrochem. Commun.* **12**, 570–573 (2010).

45. Liu, J. I., Cui, W. J., Wang, C. X. & Xia, Y. Y. Electrochemical reaction of lithium with $CoCl_2$ in nonaqueous electrolyte. *Electrochem. Commun.* **13**, 269–271 (2011).

46. Hu, Y. Y. *et al.* Origin of additional capacities in metal oxide lithium-ion battery electrodes. *Nat. Mater.* **12**, 1130–1136 (2013).

47. Li, Z. *et al.* Three-dimensional nanohybrids of Mn_3O_4/ordered mesoporous carbons for high performance anode materials for lithium-ion batteries. *J. Mater. Chem.* **22**, 16640–16648 (2012).

48. Luo, J. *et al.* Three-dimensional graphene foam supported Fe_3O_4 lithium battery anodes with long cycle life and high rate capability. *Nano Lett.* **13**, 6136–6143 (2013).

49. Ko, Y. N., Park, S. B., Jung, K. Y. & Kang, Y. C. One-pot facile synthesis of ant-cave-structured metal oxide-carbon microballs by continuous process for use as anode materials in Li-ion batteries. *Nano Lett.* **13**, 5462–5466 (2013).

50. Park, M. S., Kang, Y. M., Wang, G. X., Dou, S. X. & Liu, H. K. The effect of morphological modification on the electrochemical properties of SnO_2 nanomaterials. *Adv. Funct. Mater.* **18**, 455–461 (2008).

51. Chen, X., Zhang, N. & Sun, K. Facile fabrication of CuO mesoporous nanosheet cluster array electrodes with super lithium-storage properties. *J. Mater. Chem.* **22**, 13637–13642 (2012).

52. Chen, Y. S. *et al.* Microscopic mechanism for unipolar resistive switching behaviour of nickel oxides. *J. Phys. D: Appl. Phys.* **45**, 065303 (2012).

53. Choi, S. H. & Kang, Y. C. Yolk–Shell, hollow, and single-crystalline $ZnCo_2O_4$ Powders: preparation using a simple one-pot process and application in lithium-ion batteries. *ChemSusChem* **6**, 2111–2116 (2013).

54. Takami, N., Satoh, A., Hara, M. & Ohsaki, T. Structural and kinetic characterization of lithium intercalation into carbon anodes for secondary lithium batteries. *J. Electrochem. Soc.* **142**, 371–379 (1995).

Acknowledgments

Author contributions

G.D.P. and Y.C.K. devised the concept, designed the experiment, and wrote the manuscript. G.D.P. and Y.N.K. performed the experiments and analyzed the data. Y.C.K. supervised the project. All authors discussed the results and contributed in this manuscript.

Additional information